Precision Force Tracking Control of a Surgical Device Interacting With a Deformable Membrane

Zhao Feng, Wenyu Liang, *Member, IEEE*, Jie Ling, *Member, IEEE*, Xiaohui Xiao, *Member, IEEE*, Kok Kiong Tan, and Tong Heng Lee, *Member, IEEE*

***Abstract*—Well-designed robotic-assisted surgical systems have been widely applied in medical treatments to make surgical operations precise and efficient. For these, precise tracking of the interaction force between the surgical device and affected human tissues is an important aspect to improve the safety and surgery success rate. In this development, an adaptive integral terminal sliding mode force control scheme for a piezoelectric actuator-based ear surgical device is presented to achieve precision force tracking during the interaction with the tympanic membrane that is soft and deformable, an important aspect in the course of such a surgery. Particularly, a force error-based integral terminal sliding manifold is employed to guarantee the finite-time convergence performance. A related adaptive control law is developed and deployed to estimate the controller's parameters and update the switching gain to accommodate system uncertainties, disturbances, and the complex contact environment. Then, the stability of the proposed control method is analyzed and discussed rigorously based upon the Lyapunov theory and method. Furthermore and rather importantly, comparative experiments with three other force controllers are conducted for both S-curve and sine waves with different frequencies. The force tracking results interacting with the deformable membrane demonstrate that the best performance is achieved by the proposed method with all the statistical errors within a suitably effective range of 2.5% and 9.0% of the maximum amplitude.**

***Index Terms*—Adaptive control, medical robotics, nonlinear control.**

I. Introduction

With the high-speed development of mechatronic and robotic technologies, the advanced equipment of robotic-assisted surgical systems have been widely applied to work together with surgeons to achieve high precision, repeatability, and dexterious surgeries [1]. Many of these surgical devices for various surgical applications have been designed in recent years, such as beating heart surgery [2], single-incision laparoscopic surgery [3], minimally invasive surgery [4], orthognathic surgical robots [5], subretinal injection [6], and so on, with the benefits of less pain, hemorrhaging, trauma, and operating time.

In the field of otolaryngology, once excess fluid is accumulated in the middle ear, a prevailing disease called otitis media with effusion (OME) will arise, which may result in hearing loss and body imbalance [7]. The surgery to treat OME via tube placement, in a procedure termed myringotomy with tube insertion is essential after the first treatment if just using medication fails. The patient is usually put under general anesthesia (GA) in an operating theater so that the patient can be kept completely still during this surgery. Although it is a minor surgery, the need for GA and surgeon's skills are required to achieve safe operations. Also, another limitation of the current surgical treatment is treatment delay due to the waiting time for the operating theater. Thus, in [7], the ventilation tube applicator (VTA), a novel ear surgical device, was developed to help surgeons to conduct the surgery, providing the surgical treatments to the patients automatically or semiautomatically. The VTA aims to allow the office-based myringotomy with tube insertion without the need of GA. During the use of the VTA, the surgeon can potentially conduct the surgery with local anesthesia, moving the surgery out of the operating theater to an outpatient setting like clinic or surgeon's office. Benefiting from the advantages of the developed mechatronics system, the myringotomy with tube insertion can be done by the VTA in a safe, simple, and cost-effective way.

Different from the conventional surgery conducted by experienced surgeons, the semiauto surgical device perceives and

Manuscript received November 12, 2021; revised January 17, 2022 and March 24, 2022; accepted May 10, 2022. Recommended by Technical Editor J. A. Schultz and Senior Editor H. Qiao. This work was supported in part by the A*STAR Career Development Fund under Grant C210812049, and in part by the Natural Science Foundation of China under Grant 51375349, and in part by National Science Foundation of Jiangsu Provice of China under Grant BK20210294. *(Corresponding authors: Wenyu Liang; Xiaohui Xiao.)*

Zhao Feng is with the School of Power and Mechanical Engineering, Wuhan University, 430072, China, and also with the Department of Electrical and Computer Engineering, National University of Singapore (NUS), Singapore 117576 (e-mail: fengzhaozhao7@whu.edu.cn).

Wenyu Liang is with the Institute for Infocomm Research, A*STAR, Singapore 138632, and also with the Department of Electrical and Computer Engineering, National University of Singapore, Singapore 117576 (e-mail: liangwenyu@nus.edu.sg).

Jie Ling is with the College of Mechanical & Electrical Engineering, Nanjing University of Aeronautics and Astronautics, Nanjing 210016, China (e-mail: meejling@nuaa.edu.cn).

Xiaohui Xiao is with the School of Power and Mechanical Engineering, Wuhan University, Wuhan 430072, China (e-mail: xhxiao@whu.edu.cn).

Kok Kiong Tan is with ZAI Company, Singapore (e-mail: eletankk@gmail.com).

Tong Heng Lee is with the Department of Electrical and Computer Engineering, National University of Singapore, Singapore 117576 (e-mail: eleleeth@nus.edu.sg).

Color versions of one or more figures in this article are available at https://doi.org/10.1109/TMECH.2022.3177792.

Digital Object Identifier 10.1109/TMECH.2022.3177792

plans the operating processes by the force and position sensors. Therefore, during the touch phase of this procedure, it is necessary to track the interaction/contact force between the grommet tube put on the surgical device and the deformable membrane as precisely as possible. This force should be kept within a clearly prescribed acceptable level so that the device can execute the myringotomy procedure with a high success rate. Certainly here too, noting that this is essentially a type of surgical procedure with the semiauto surgical device, the requisite great care needs to be taken as it may cause hearing loss if the force exerted on the tympanic membrane (TM) is inappropriate, or causes some attendant resultant undesirable trauma on the deformable membrane [7], [8]. As a consequence, the contact force applied on the membrane should be controlled and tracked accurately to achieve desirable outcomes.

For such force trajectory tracking, in [9], a force control based on the proportional–integral–derivative (PID) methodology was developed to improve the success rate compared with position-based control only. There, because a motion controller is entwined in the control scheme, the tracking bandwidth is unfortunately limited seriously. Alternatively, constructing the relationship between surgical devices and environment is an effective method to improve the force tracking performance substantially. Thus commonly, the environment is typically considered as a linear elastic material for the controller design in various suitably interesting work available in the published literature [10]. These methods are generally effective and easy to be implemented, and applicable under situations of contact with largely rigid materials. However, for the case of soft human tissues (such as TM), it is essential to note that these are usually viscoelastic, nonlinear, and inhomogeneous; which would bring great challenges for appropriate and effective controller design [11], [12].

In various relevant works, say, for example, in [13], a force control strategy on basis of a cell model utilizing polynomial functions and the feedback linearization technique was proposed to achieve an explicit force tracking for a cell injection system. Further, in [14], an adaptive force tracking control strategy was proposed using a Kelvin–Boltzmann model with numerical studies. To improve the performance of the force controller, an active observer with the Kelvin Boltzmann interaction model has been presented with experimental validation in [15]. In addition, the constrained linear-quadratic optimized PID controller integrating with a disturbance observer (DOB) was developed on basis of the standard linear solid contact model for optimal contact force control, and this is implemented and used in an ear surgical device in [16]. It is noteworthy that the utilized viscoelastic models in the aforementioned earlier works are all linear so that they can be integrated into these controllers easily. This is essentially attained through establishing a linear relationship between the control input and the measured force. However, according to further studies in [8], the Hunt–Crossley nonlinear model is likely more appropriate to be used to better and more accurately model the soft materials of human tissues and deformable objects. This is essential to be aware; because it can arise that due to the inaccurate description of the underlying environment in the various existing methods, the response of the force control system can be significantly limited. Nevertheless, although such a model-based force control utilizing the Hunt–Crossley model was indeed developed and applied to robot-assisted minimally invasive surgery in [17], it needs to be noted that this method there can only track the step response due to the utilization of a possibly constraining local linearization of the nonlinear model. Thus, efforts to utilize the Hunt–Crossley nonlinear model have also been limited. Additionally, in other noteworthy recent interesting works, a method of a direct force tracking controller was described in [18] to achieve rapid force rise times and applied to variable physical damping actuator contacting with rigid environment. The method there is a model-free sliding-mode force tracking control using time-delayed estimation technology.

For piezoelectric actuator-based ear surgical devices, although there are certainly great potential and possibilities, a considerable challenge is in the nonlinearities such as nonlinear friction that exists inherently in the piezoelectric actuator. Apart from this, the parametric uncertainties and other modeling uncertainties also need to be compensated. To avoid the complex and time-consuming modeling of nonlinearities, a DOB-based sliding-mode control was developed in [19], and a neural-network-based learning controller was designed for a nanopositioning system in [20]. Additionally, the approach of integral sliding-mode control was proposed in [21], and that with adaptive law was proposed in [22], respectively. It should also be noted that the surgical operation should be conducted as quickly as possible to relieve the pain of the patients, thus the fast convergence performance is also important. For these, while exhibiting great potential, nevertheless finite-time convergence performance was not attained in their outcomes. Moreover, these controllers were designed for precision position tracking primarily; and the designs thus did not attempt to consider force information when contacting with the deformable membrane, which would have required a significantly more complex environment modeling and consideration also of uncertainties.

Motivated by the aforementioned important issues and considering also model uncertainty and unknown disturbances, in the work here, the approach taken is first to build a more appropriate system dynamic model incorporating component terms of nonlinearities (e.g., friction), undesired and unknown disturbances, as well as interaction with the deformable membrane environment. Then, a novel adaptive integral terminal sliding-mode force control (AITSMFC) is developed for desired force trajectory tracking. The stability analysis on the proposed control system is carried out rigorously based on the well-known Lyapunov theory and method. Finally, different and extensive experiments on the piezoelectric actuator-based ear surgical device are performed to verify the tracking performance of the force control on a soft deformable mock membrane through comparisons. In this article, thus, the main contributions include the following:

1) A force error-based integral terminal sliding-mode function is designed and developed to achieve both precision steady-state performance and finite-time convergence so

that the explicit force tracking controller is implemented without the need to especially and precisely model the contact environment, which is particularly suitable (and actually also rather efficacious in practice) for the contact environment of soft tissues exhibiting strong nonlinearity and uncertainty.

2) An adaptive control law is also analytically deduced and constructed to estimate the controller's parameters as well as update the switching gain online to improve the robustness to undesired disturbances and relieve chattering phenomenon to further enhance the precision.
3) Various experiments of force tracking on a soft deformable mock membrane are conducted to check the controller's performance on the actual surgical device.

The rest of this article is organized as follows. The model of the piezoelectric actuator-based robot-assisted surgical system is presented in Section II. Next, the detailed design and the stability analysis of the proposed control method are provided in Section III. Then, in Section IV, the experimental system as well as the parameters of different controllers are presented. Section V elaborates the experiments on the surgical device as well as comparison results. Finally, Section VI concludes this article.

II. System Model of the Surgical Device

A surgical device developed in earlier work in [7] is appropriately driven by a ultrasonic piezoelectric motor (USM) that is on the basis of the piezoelectric effect. At this point, it is also appropriate to mention that the motivation of the work in this article is based on observations in our work in collaboration with the Department of Otolaryngology, National University of Singapore (NUS). For this effort, there has been the involvement of an experienced ENT (ear, nose, and throat) surgeon; and development of the system has been in collaboration with this Department of Otolaryngology, NUS. The surgical device now further developed and introduced in this article is an instance of a semiautomated surgical device that will substantially further assist the surgeon to complete the required surgical process of myringotomy with tube insertion; and at one go automatically, safely, and precisely.

This surgical device is mainly designed to conduct ear surgeries on the eardrum. Generally, for modeling the USM, a second-order system can represent the USM dynamics as

$$m\ddot{x} + b\dot{x} + kx + f_n + f_{\text{ud}} = Tu \tag{1}$$

where x denotes the motor output position, and $\dot{x}$ and $\ddot{x}$ are the velocity and acceleration of the motor, respectively. m, b, and k are the effective mass, the effective damping coefficient, and the effective stiffness, respectively. The variable u is the control input voltage and T denotes a parameter related to the system electromechanical ratio. f_n is the nonlinear term including friction inherently in the USM in practice. f_{ud} is the undesired disturbances, such as heat disturbance due to the driving principle of the USM, unmodeled dynamics, and unknown relative motion between the toolset and eardrum. During the operation process, the piezoelectric actuator-based ear surgical device should contact with the deformable membrane so that the end effector is exerted on an interaction force. Accordingly, Fig. 1 demonstrates the practical diagram for the surgical device when contacting with environment, where the dynamics is expressed as

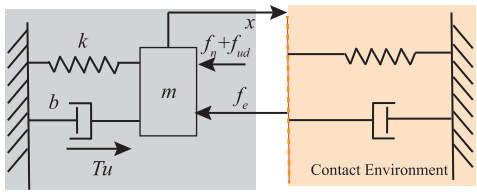

Fig. 1. Block diagram of the model of the surgical device with unknown soft contact environment.

$$m\ddot{x} + b\dot{x} + kx + f_n + f_{\text{ud}} + f_e = Tu \tag{2}$$

where f_e denotes the interaction force between the device and environment. It should be noted that f_n and f_{ud} always exists in this system because of the driving principle and mechanical structure of USM, while f_e occurs only during contact.

Assumption 1: [23] The f_n and f_{ud} are bounded as follows:

$$|f_n| \le \delta f_n, |f_{\text{ud}}| \le \delta f_{\text{ud}} \tag{3}$$

where δf_n and δf_{ud} are both positive constants.

In practice, the accurate mathematical model of the surgical device is difficult to be obtained. In order to consider this aspect, the parameters' uncertainties are introduced as

$$\Delta m = m - m_n, \Delta b = b - b_n, \Delta k = k - k_n \tag{4}$$

where m_n, b_n, and k_n are the nominal or identified parameters and Δm, Δb, and Δk represent the parametric errors, respectively, which are bounded by δm, δb, and δk. Therefore, the dynamics of this system can be rewritten as

$$m_n\ddot{x} + b_n\dot{x} + k_n x + \Theta + f_n + f_{\text{ud}} + f_e = Tu \tag{5}$$

where $\Theta = \Delta m\ddot{x} + \Delta b\dot{x} + \Delta kx$.

Assumption 2: [24] The model uncertainties Θ are bounded by

$$|\Theta| \le \delta_m|\ddot{x}| + \delta_b|\dot{x}| + \delta_k|x| = \delta_\Theta \tag{6}$$

where $\delta_\Theta > 0$ is a constant.

According to the aforementioned assumptions, the total disturbance $f_t = f_n + f_{\text{ud}} + \Theta$ is also bounded as

$$|f_t| \le \delta f_t = \delta f_n + \delta f_{\text{ud}} + \delta_\Theta \tag{7}$$

where δf_t is a parameter that is unknown. Therefore, the dynamics shown in Fig. 1 is simplified as

$$m_n\ddot{x} + b_n\dot{x} + k_n x + f_t + f_e = Tu. \tag{8}$$

Thus, the objective of this article is to make sure the measured force f_e to track the desired contact force f_d accurately and precisely at the presence of total disturbance f_t under unknown contact environment.

Remark 1: In this article, to simplify controller's design, the friction, model uncertainties, and other undesired disturbance

are bounded by positive values. These assumptions have also been widely used elsewhere, in research and development work on piezoelectric-actuated devices in, say, [23]–[25]. The unknown term is treated as a lumped disturbance to avoid complex modeling frictions, and in fact (in reality in any case) there always exists an upper bound for a practical system. The robustness of the designed controller to these adverse impacts is an important aspect to be taken into consideration in this article to achieve appropriately effective performance.

III. Design of Adaptive Integral Terminal Sliding-Mode Force Control

As mentioned previously, the precision force tracking is of vital importance for the surgical device. Hence, the aim of the control scheme to be designed is to minimize the force tracking error during the contact with environment defined as

$$e_f = f_d - f_e \tag{9}$$

where f_d is the desired force trajectory.

A. Integral Terminal Sliding-Mode Force Controller

For the purpose of facilitating the controller design, the system dynamics, i.e., (8), is rewritten as

$$\eta_n + f_t + f_e = Tu \tag{10}$$

where $\eta_n = m_n\ddot{x} + b_n\dot{x} + k_n x$ denotes the model information related to position. To obtain better robustness and steady-state performance, the integral action is necessary in the sliding function, and the fractional-order term of the sign error guarantees the finite-time convergence performance [26]. Therefore, a force error-based integral terminal sliding manifold is given by

$$s = e_f + \sigma_1 \int_0^t [e_f(\tau) + \sigma_2 \mathrm{sig}(e_f)^\rho]\, d\tau \tag{11}$$

where

$$\mathrm{sig}(\cdot)^\rho = |\cdot|^\rho \mathrm{sign}(\cdot) \tag{12}$$

and $\sigma_1 > 0, \sigma_2 > 0, 0 < \rho < 1$. It should be noted that although the sliding manifold contains the switching term sign, the function $\mathrm{sig}(\cdot)^\rho$ as well as the sliding function is continuous and differentiable. Then, the time derivative of s can be given as

$$\dot{s} = \dot{e}_f + \sigma_1 e_f + \sigma_1\sigma_2 \mathrm{sig}(e_f)^\rho. \tag{13}$$

Consider the following equation as the Lyapunov candidate function:

$$V_e = \frac{1}{2} e_f^2 \tag{14}$$

and through deriving it with respect to time, $\dot{V}_e$ is

$$\dot{V}_e = e_f \dot{e}_f. \tag{15}$$

In the sliding motion, $\dot{s} = 0$ is produced, and hence, $\dot{e}_f$ is given by

$$\dot{e}_f = -\sigma_1 e_f - \sigma_1\sigma_2 \mathrm{sig}(e_f)^\rho. \tag{16}$$

Then, the following equation can be obtained:

$$\begin{aligned}\dot{V}_e &= e_f[-\sigma_1 e_f - \sigma_1\sigma_2 \mathrm{sig}(e_f)^\rho] \\ &= -\sigma_1 e_f^2 - \sigma_1\sigma_2 |e_f|^{\rho+1} = -\sigma_1 e_f^2 - \sigma_1\sigma_2 (e_f^2)^{\frac{\rho+1}{2}} \le 0.\end{aligned} \tag{17}$$

And we can rewrite the aforementioned equation as

$$\dot{V}_e + aV_e + bV_e^c \le 0 \tag{18}$$

where $a = 2\sigma_1, b = 2^{\frac{\rho+1}{2}}\sigma_1\sigma_2$, and $c = \frac{\rho+1}{2}$. Hence, the convergence occurs in finite time T_s [27], which is as follows:

$$T_s \le \frac{1}{a(1-c)} \ln \frac{aV_{e,0}^{1-c} + b}{b} \tag{19}$$

where the initial value of V_e in (14) is defined as $V_{e,0}$.

Theorem 1: For the system presented in (10), the error e_f converges to zero in a finite time with the sliding manifold (11), while the following integral terminal sliding-mode force control law is applied:

$$u = T^{-1}\eta_n + T^{-1}[f_d + \sigma_1^{-1}\dot{e}_f + \sigma_2 \mathrm{sig}(e_f)^\rho + \lambda \mathrm{sign}(s)] \tag{20}$$

where λ is the switching gain and it satisfies

$$\lambda > \delta f_t + \epsilon \tag{21}$$

and ϵ is an arbitrary positive constant.

Proof of Theorem 1: A Lyapunov candidate function V_1 for the integral terminal sliding-mode force control is given by

$$V_1 = \frac{1}{2} s^2. \tag{22}$$

The time derivative of V_1 is

$$\dot{V}_1 = s\dot{s}. \tag{23}$$

Substituting (13) into (23), we have

$$\dot{V}_1 = s[\dot{e}_f + \sigma_1 e_f + \sigma_1\sigma_2 \mathrm{sig}(e_f)^\rho]. \tag{24}$$

According to (10), it is obtained that

$$f_e = Tu - \eta_n - f_t \tag{25}$$

and substituting it into (9), yields

$$e_f = f_d - (Tu - \eta_n - f_t). \tag{26}$$

Therefore, the following expression is generated:

$$\dot{V}_1 = s[\dot{e}_f + \sigma_1\sigma_2 \mathrm{sig}(e_f)^\rho + \sigma_1 f_d - \sigma_1 Tu + \sigma_1\eta_n + \sigma_1 f_t]. \tag{27}$$

Substituting the control law (20) into (27) gives

$$\begin{aligned}\dot{V}_1 &= s[\dot{e}_f + \sigma_1\sigma_2 \mathrm{sig}(e_f)^\rho + \sigma_1 f_d - \sigma_1\eta_n - \sigma_1 f_d - \dot{e}_f \\ &\quad - \sigma_1\sigma_2 \mathrm{sig}(e_f)^\rho - \sigma_1\lambda \mathrm{sign}(s)) + \sigma_1\eta_n + \sigma_1 f_t] \\ &= s[-\sigma_1\lambda \mathrm{sign}(s) + \sigma_1 f_t] \\ &= -\sigma_1 |s|[\lambda - f_t \mathrm{sign}(s)].\end{aligned} \tag{28}$$

If (21) is satisfied, we can obtain

$$\dot{V}_1 < -\sigma_1 |s| \epsilon < -\sqrt{2}\sigma_1 \epsilon V_1^{\frac{1}{2}} < 0. \tag{29}$$

Thus, it can be guaranteed that the control law is stable within a finite time, and once $\dot{V}_1 \to 0$, a finite-time force error convergence will achieve after the sliding mode is reached by the system [28]. □

B. Adaptive Parameters Design

It is clear that the control law (20) is based on the known parameters, i.e., m_n, b_n, and k_n. However, in practice, these parameters need to be obtained accurately enough to improve the force tracking performance. Sometimes, system parameters are even unknown. If the parameters' uncertainties in (4) and (5) are too large, λ would also be large enough to retain stability, subsequently leading to unexpected oscillation near the sliding-mode manifold. Additionally, the selection of the switching gain λ is calculated according to the upper bound of the total disturbance δf_t. Generally, the gain is selected as a large one to ensure the stability because the bound is unknown in practice, which would degrade the force tracking precision. To overcome these issues, an adaptive methodology to alleviate this problem is incorporated into the integral terminal sliding-mode force control, i.e., AITSMFC in this section to achieve fast and precision force tracking.

For a clear expression, the term containing the actual system parameters is expressed as

$$\eta = m\ddot{x} + b\dot{x} + kx \tag{30}$$

and the errors between the actual and estimated parameters are defined by the following:

$$\tilde{m} = \hat{m} - m,\ \tilde{b} = \hat{b} - b, \tilde{k} = \hat{k} - k \tag{31}$$

where $\hat{m}$, $\hat{b}$, and $\hat{k}$ are the estimations of the parameters m, b, and k, respectively. Furthermore, the estimation error for the desired switching gain λ_d is also introduced as

$$\tilde{\lambda} = \hat{\lambda} - \lambda_d. \tag{32}$$

Theorem 2: For the system shown in (8), the force error e_f will converge to zero while applying the AITSMFC to the system

$$u = T^{-1}\hat{\eta} + T^{-1}[f_d + \sigma_1^{-1}\dot{e}_f + \sigma_2 \mathrm{sig}(e_f)^\rho + \hat{\lambda}\mathrm{sign}(s)] \tag{33}$$

where $\hat{\eta} = \hat{m}\ddot{x} + \hat{b}\dot{x} + \hat{k}x$ is with the adaptive control laws as shown in the following:

$$\dot{\hat{\lambda}} = \sigma_1|s|, \quad \dot{\hat{m}} = P_m s\sigma_1\ddot{x}$$
$$\dot{\hat{b}} = P_b s\sigma_1\dot{x}, \quad \dot{\hat{k}} = P_k s\sigma_1 x \tag{34}$$

where P_m, P_b, and P_k are constant positive parameters of the adaptive rules.

Proof of Theorem 2: For the stability evaluation on the proposed control law, a continuous and nonnegative Lyapunov candidate function is defined as

$$V = V_1 + V_2 + V_3 \tag{35}$$

where V_1 is given by (22), and V_2 and V_3 are defined as

$$V_2 = \frac{1}{2}\tilde{\lambda}^2 \tag{36}$$

$$V_3 = \frac{1}{2P_m}\tilde{m}^2 + \frac{1}{2P_b}\tilde{b}^2 + \frac{1}{2P_k}\tilde{k}^2. \tag{37}$$

Therefore, $\dot{V}_1$ becomes

$$\begin{aligned}\dot{V}_1 &= s[\dot{e}_f + \sigma_1\sigma_2 \mathrm{sig}(e_f)^\rho + \sigma_1 f_d - \sigma_1 f_e] \\ &= s[\dot{e}_f + \sigma_1\sigma_2 \mathrm{sig}(e_f)^\rho + \sigma_1 f_d - \sigma_1 Tu + \sigma_1\eta + \sigma_1 f_t)].\end{aligned} \tag{38}$$

Taking the control law (33) into the aforementioned equation, we can obtain that

$$\begin{aligned}\dot{V}_1 &= s\sigma_1(\eta - \hat{\eta}) + s[-\sigma_1\hat{\lambda}\mathrm{sign}(s) + \sigma_1 f_t] \\ &= s\sigma_1(m - \hat{m})\ddot{x} + s\sigma_1(b - \hat{b})\dot{x} + s\sigma_1(k - \hat{k})x \\ &\quad + s[-\sigma_1\hat{\lambda}\mathrm{sign}(s) + \sigma_1 f_t] \\ &= -s\sigma_1\tilde{m}\ddot{x} - s\sigma_1\tilde{b}\dot{x} - s\sigma_1\tilde{k}x \\ &\quad + s[-\sigma_1\hat{\lambda}\mathrm{sign}(s) + \sigma_1 f_t].\end{aligned} \tag{39}$$

The time derivative of V_2 is

$$\dot{V}_2 = \tilde{\lambda}\dot{\tilde{\lambda}} = \sigma_1|s|\tilde{\lambda} \tag{40}$$

and the time derivative of V_3 is

$$\dot{V}_3 = \frac{\tilde{m}}{P_m}\dot{\tilde{m}} + \frac{\tilde{b}}{P_b}\dot{\tilde{b}} + \frac{\tilde{k}}{P_k}\dot{\tilde{k}}. \tag{41}$$

Finally, $\dot{V}$ can be obtained by the following combination:

$$\begin{aligned}\dot{V} &= \dot{V}_1 + \dot{V}_2 + \dot{V}_3 \\ &= -s\sigma_1\tilde{m}\ddot{x} - s\sigma_1\tilde{b}\dot{x} - s\sigma_1\tilde{k}x + s[-\sigma_1\hat{\lambda}\mathrm{sign}(s) \\ &\quad + \sigma_1 f_t] + \sigma_1|s|\tilde{\lambda} + \frac{\tilde{m}}{P_m}\dot{\tilde{m}} + \frac{\tilde{b}}{P_b}\dot{\tilde{b}} + \frac{\tilde{k}}{P_k}\dot{\tilde{k}} \\ &= \tilde{m}\left(-s\sigma_1\ddot{x} + \frac{\dot{\hat{m}}}{P_m}\right) + \tilde{b}\left(-s\sigma_1\dot{x} + \frac{\dot{\hat{b}}}{P_b}\right) \\ &\quad + \tilde{k}\left(-s\sigma_1 x + \frac{\dot{\hat{k}}}{P_k}\right) + s[-\sigma_1\hat{\lambda}\mathrm{sign}(s) + \sigma_1 f_t] + \sigma_1|s|\tilde{\lambda} \\ &= s[-\sigma_1\hat{\lambda}\mathrm{sign}(s) + \sigma_1 f_t] + \sigma_1|s|(\hat{\lambda} - \lambda_d) \\ &= -\sigma_1|s|[\lambda_d - f_t\mathrm{sign}(s)] < -\sigma_1|s|\epsilon < 0.\end{aligned} \tag{42}$$

After the adaption time, the gains $\hat{\lambda}, \hat{m}, \hat{b}$, and $\hat{k}$ attain their desired values, respectively, and the estimation errors $\tilde{\lambda}, \tilde{m}, \tilde{b}$, and $\tilde{k}$ vanish. The Lyapunov function (35) becomes

$$V = \frac{1}{2}s^2. \tag{43}$$

According to (43), it is derived from (42) that

$$V + \sqrt{2}\sigma_1\epsilon V^{\frac{1}{2}} < 0. \tag{44}$$

Therefore, the convergence of s occurs in finite time [27]. Then, the finite-time force error convergence will achieve after the sliding mode is reached by the system [28], and the proposed AITSMFC ensures the zero steady-state tracking error. □

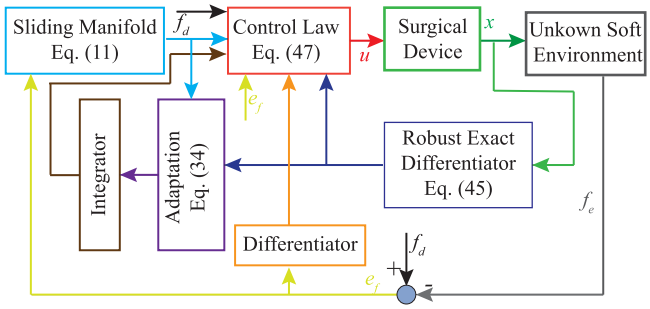

Fig. 2. Block diagram of the proposed AITSMFC.

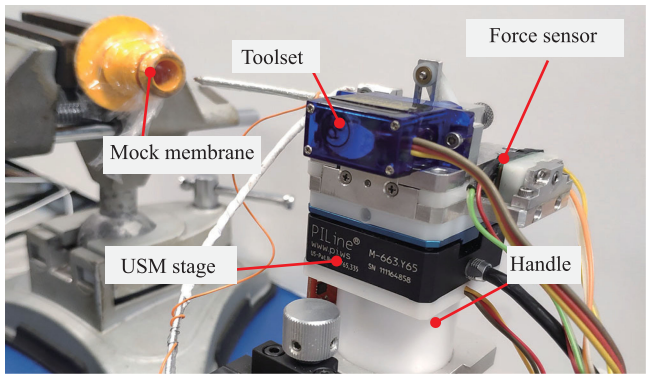

Fig. 3. Experimental system using the surgical device.

C. Overall Control Law

The calculation of high-order derivatives, $\ddot{x}$ and $\dot{x}$, is necessary to implement the proposed AITSMFC. To obtain a finite-time convergence of the system states and alleviate the impact of noise, the robust exact differentiator (RED) [29], [30] is utilized. A second-order RED is expressed as

$$\begin{aligned}\dot{z}_0 &= v_0 = -\lambda_1|z_0 - x|^{\frac{2}{3}}\text{sign}(z_0 - x) + z_1\\ \dot{z}_1 &= v_1 = -\lambda_2|z_1 - z_0|^{\frac{1}{2}}\text{sign}(z_1 - v_0) + z_2\\ \dot{z}_2 &= -\lambda_3\text{sign}(z_2 - v_1)\end{aligned} \tag{45}$$

where $z_0 = \hat{x}$, $z_1 = \dot{\hat{x}}$, $z_2 = \ddot{\hat{x}}$ and the parameters should satisfy $\lambda_1 = 3\lambda_0^{\frac{1}{3}}$, $\lambda_2 = 1.5\lambda_0^{\frac{1}{2}}$, and $\lambda_3 = 1.1\lambda_0$ with $\lambda_0 \geq |\dddot{x}|$.

To further alleviate the discontinuity of the sign function $\text{sign}(s)$, a boundary layer technique presented in [31] is applied, where a saturation function defined in (46) replaces the discontinuous function

$$\text{sat}\left(\frac{s}{\phi}\right) = \begin{cases}\text{sign}(s), & \text{if } |s| > \phi\\ \frac{s}{\phi}, & \text{if } |s| \leq \phi\end{cases} \tag{46}$$

where the ϕ is a positive constant that is the boundary layer thickness to ensure s bounded by ϕ. As a result, the overall control law is written as

$$\begin{aligned}u = T^{-1}\Big[&\hat{m}\ddot{\hat{x}} + \hat{b}\dot{\hat{x}} + \hat{k}\hat{x}\\ &+ f_d + \sigma_1^{-1}\dot{e}_f + \sigma_2\text{sig}(e_f)^{\rho} + \hat{\lambda}\text{sat}\left(\frac{s}{\phi}\right)\Big]\end{aligned} \tag{47}$$

and Fig. 2 depicts the detailed block diagram of the proposed AITSMFC.

Remark 2: In practical situations, the presence of sensor measurement noise is an essentially inevitable matter. Certainly thus, and on article at least for the integral action of the adaptive law, the presence of this sensor measurement noise may possibly result in unbounded values in the associated numerical computations. In general though, this is a rather well-known problem and can be directly and straightforwardly alleviated by the commonly used dead-zone technique [28], [32] or projection operator [33] for the actual experiment.

Remark 3: In [34] and [35], the integral sliding-mode controllers are designed to realize precision tracking. However, the about methods cannot involve the finite-time convergence performance for the liner sliding function, and the design procedures require the accurate model parameters. In this article, the integral terminal sliding manifold ensures the convergence is achieved in finite time, and the adaptive law handles the unknown disturbance and the model uncertainties so that the robustness is improved significantly.

Remark 4: It is noteworthy that being different from the methods in [21], [34], and [35] aiming at precision position tracking, the aim of this article is to achieve accurate and precise force tracking under soft environment, which is usually viscoelastic, nonlinear, and inhomogeneous [12], giving rise to more uncertainties and challenges on controller's design in comparison with rigid contact in [18], [36]. Moreover, the proposed method can track force trajectory without accurately modeling the contact environment, which is unlike to the force tracking controllers proposed in [14]–[17], and [37], and thus, simplify the implementation, especially for the interaction with soft human tissues. Besides, the proposed controller can also deal with the same conditions in common position tracking, such as friction, and unknown system parameters existing in the piezoelectric actuator-based ear surgical device.

IV. Experimental Setup

A. Experimental System

To evaluate the force tracking performance, an experimental system using the piezoelectric actuator-based ear surgical device is illustrated in Fig. 3. In general, the average elastic modulus of human TM is in the range of 100–300 MPa [38], the thickness is 30–120 μm [39], [40]. Due to the similar mechanical properties of polyethylene (PE) with the average elastic modulus of 225 MPa, thickness of about 50–100 μm, the PE film is employed as the soft deformable mock membrane to enable a controlled calibration of system performance in this work. Furthermore, in [41], a force-sensing myringotomy was used to measure the strength of human TM, the results of which show that the peak load at breakage ranges from 0.011 to 0.443 N. Here, the cutting force on the PE membrane by using a myringotomy knife is tested, which shows an average peak cutting force of 0.13

± 0.04 N. Therefore, it can be noted that the cutting strength of the mock membrane is appropriately within the range of the associated human TM's cutting strength. The PE membrane thus can be affirmed to have similar characteristics to the human TM. A Physik Instrumente PI-M663 USM stage is employed to move the toolset mounted on the device to get into contact with the soft deformable membrane. A Honeywell FS1500NS force sensor is used to measure the information arising from physical interaction between the surgical device and the contacting environment (i.e., membrane). A computer installed with a dSPACE DS1104 control card is utilized to receive the sensor outputs from the device via quadrature encoder pulse (QEP) module and analog-to-digital converter, implement the force control system, as well as send out the control signal to the Physik Instrumente PI Line C-867 Motion Controller via a digital-to-analog converter in order to control the surgical device. The real-time control system is built via the MATLAB/Simulink blocks. The sampling time of the overall control system is 1 ms. Furthermore, a multi-frequencies square wave is injected into the USM stage without contacting with the environment to obtain the nominal plant for facilitating the controller design, and the linear term [16] is identified through the MATLAB system identification toolbox as

$$\ddot{x} + 248.4\dot{x} + 202x = 4940\,u. \tag{48}$$

B. Controllers Implementation

For the purpose of verifying the effectiveness and performance of the proposed control scheme, the comparative tests are conducted using the following four controllers: PI controller [16], model-based integral terminal sliding-mode force control (MBITSMFC), model-free integral terminal sliding-mode force control (MFITSMFC) [18], and the proposed AITSMFC.

For the PI controller, the parameters are set as $K_p = 8$, $K_i = 0.05$, and a disturbance observer with a bandwidth 150 Hz is also added to improve the performance [16]. Additionally, the integral terminal sliding-mode force control on the basis of the identified model is also tested. The control law of MBITSMFC is given by

$$\begin{aligned} u_{\mathrm{MB}} = T^{-1}[&(m_n\hat{\ddot{x}} + b_n\hat{\dot{x}} + k_n\hat{x}) \\ &+ f_d + \sigma_1^{-1}\dot{e}_f + \sigma_2 \mathrm{sig}(e_f)^{\rho} + \lambda \mathrm{sat}(s/\phi)]. \end{aligned} \tag{49}$$

In [18], an MFITSMFC was also proposed through time-delayed estimation to avoid system modeling for force tracking, which is expressed as

$$\begin{aligned} u_{\mathrm{MF}} = u_{\mathrm{MF},(t-t_s)} - T^{-1} f_{s,(t-t_s)} + T^{-1}[&f_d \\ &+ \sigma_1^{-1}\dot{e}_f + \sigma_2 \mathrm{sig}(e_f)^{\rho} + k_1 s + k_2 \mathrm{sig}(s)] \end{aligned} \tag{50}$$

where the subscript of $(t - t_s)$ represents its value at the delayed time of t_s.

Table I lists all the controller parameters, where all these parameters have given the proper anticipated performance through experiments to ensure suitably fair comparison of outcomes.

TABLE I
PARAMETERS OF DIFFERENT CONTROLLERS

Parameter	MBITSMFC Eq. (49)	MFITSMFC Eq. (50)	AITSMFC Eq. (47)
σ_1	0.1	0.1	0.1
σ_2	500	50	500
ρ	0.1	0.2	0.1
λ	10	-	-
λ_0	500	-	500
ϕ	0.02	-	0.02
k_1, k_2	-	0.1	-
P_m, P_b, P_k	-	-	100

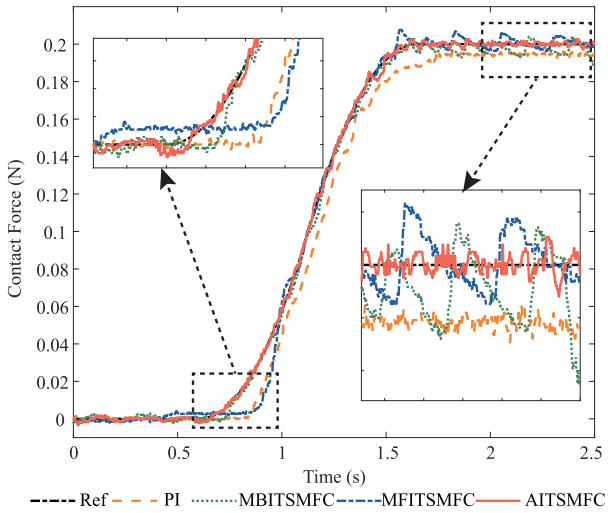

Fig. 4. Experimental results on force tracking of S-curve using different controllers.

V. RESULTS AND DISCUSSIONS

A. Force Tracking of the S-Curve

During the contact phase of the operating processes, a constant force should be exerted on the membrane. Therefore, according to the aforementioned control laws and the controllers' parameters, a commonly used force S-curve is tracked for different controllers first, which is expressed as

$$f_d = A \cdot f_{\mathrm{scurve}}(t; a, b) \tag{51}$$

where A is the steady-state value, and $f_{\mathrm{scurve}}(t; a, b)$ is the normalized S-curve defined as

$$f_{\mathrm{scurve}}(t; a, b) = \begin{cases} 0, & t \le a \\ 2\left(\frac{t-a}{b-a}\right), & a \le t \le \frac{a+b}{2} \\ 1 - 2\left(\frac{t-b}{b-a}\right), & \frac{a+b}{2} \le t \le b \\ 1, & t \ge b \end{cases} \tag{52}$$

where a and b are the start and end time of the transitional process. In the experiment, the trajectory starts at $a = 0.6$ s, achieves the amplitude of $A = 0.2$ N at $b = 1.6$ s, and maintains this value to make a constant force interaction with the mock membrane. The reference (Ref) as well as the experimental results on force tracking are plotted in Fig. 4. It can be observed from the rising process shown in the figure, the proposed AITSMFC

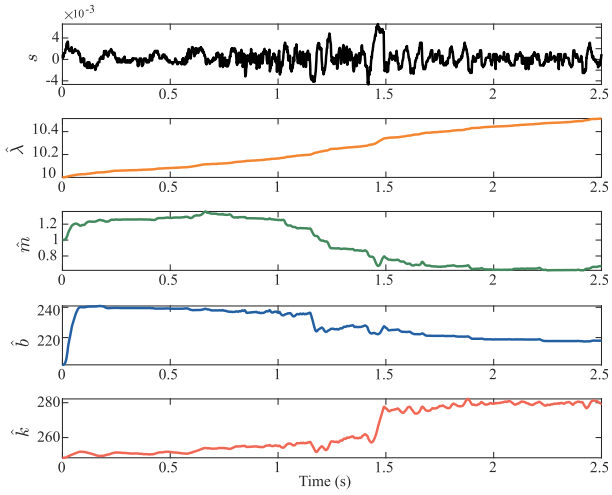

Fig. 5. Evolution of $s, \hat{\lambda}, \hat{m}, \hat{b}$, and $\hat{k}$ for the S-curve with AITSMFC.

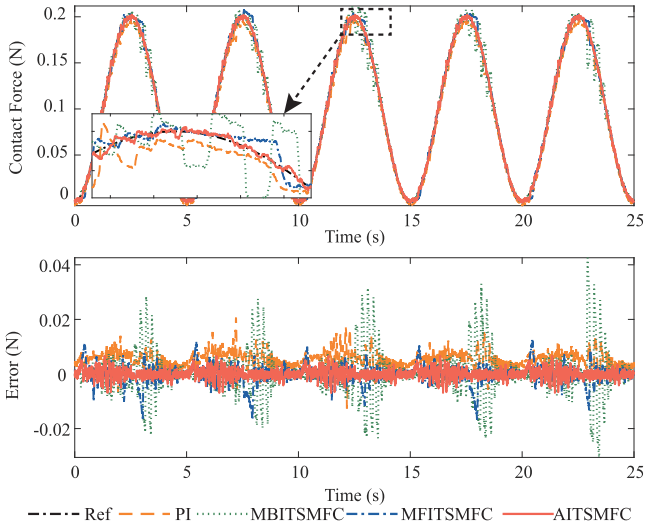

Fig. 6. Experimental results on force tracking at 0.2-Hz sine wave using different controllers.

and MBITSMFC response faster than PI and MFITSMFC as is indicated in the zoomed-in plot in Fig. 4. Moreover, for the steady-state force tracking performance after 1.6 s, the PI cannot achieve the target value in such soft environment only with the root-mean-square error (e_{rms}) of 0.0055 N and the maximal absolute error (e_{max}) of 0.0073 N, respectively. For both MBITSMFC and MFITSMFC with the e_{max} of 0.0112 and 0.0058 N, respectively, the chattering phenomenon is obvious in comparison with AITSMFC during the steady-state status. The proposed AITSMFC performs the best force tracking performance with e_{rms} of 0.001 N and e_{max} of 0.0030 N, whose errors are reduced more than 50% compared with MBITSMFC and MFITSMFC. Note that although the chattering phenomenon still exists in comparison with the PI controller, it is alleviated greatly through implementing the proposed controller, and the tracking performance is also improved significantly. The results show that the accurate and precise force tracking of the S-curve with fast response can be achieved by the proposed AITSMFC effectively.

The sliding surface s and time histories of the adaptation process of $\hat{\lambda}, \hat{m}, \hat{b}$, and $\hat{k}$ for S-curve with AITSMFC are demonstrated in Fig. 5. It can be observed that the parameters are updated automatically during the tracking process, which presents a better performance than the other controllers under model uncertainties and external disturbances. The value of $\hat{\lambda}$ increases slowly due to the small s, and the projection operator is adopted to avoid the unlimited increase. In addition to s, the values of $\hat{m}, \hat{b}$, and $\hat{k}$ are adjusted by the measured position, velocity, and acceleration, respectively. Thus, at the steady state of the S-curve, the adaptive parameters converge to about 0.7, 218, and 278, respectively, which are slightly different from the nominal values due to the identification errors and unexpected disturbances.

B. Force Tracking of Sine Waves

To test the dynamic performance of the controller interacting with a deformable object, the force tracking performances for sine waves given by

$$f_d = A \cdot \left(\frac{1 - \cos(2\pi f_s t)}{2} \right) \tag{53}$$

at different frequencies of $f_s = 0.2, 0.5, 1$ Hz with the same amplitude of $A = 0.2$ N are carried out, respectively, to evaluate the capability of the developed method in this subsection. Fig. 6 shows the tracking results at a slower speed, i.e., 0.2 Hz. It is observed that MBITSMFC produces the worst performance with e_{rms} of 0.0083 N and e_{max} of 0.0426 N for the model uncertainties during interaction process and the chattering phenomenon is evident at the peak of the tracking trajectory. The result of PI is better than MBITSMFC and with a smoother trajectory. For MFITSMFC and the proposed AITSMFC, the e_{rms} are 0.0034 and 0.0023 N, and the e_{max} are 0.0168 and 0.0087 N, which demonstrates the proposed method improves the tracking accuracy by 32.35% and 48.21%, respectively.

For the force tracking results at 0.5-Hz sine wave shown in Fig. 7, it is evident that MFITSMFC shows a relatively large force error in terms of e_{rms} and e_{max}, which are 0.0233 and 0.0874 N, respectively. The locations of the worst performance are mainly at the peak and trough of the tracking trajectory, where the friction is evident for the piezoelectric actuator-based ear surgical device [7]. However, the time-delayed estimation used in MFITSMFC cannot compensate the sudden change of friction so that there is a significant deterioration in the performance. Specifically, the PI control, MBITSMFC and AITSMFC create the e_{rms} of 0.0079, 0.0039, and 0.0026 N, respectively. Meanwhile, the e_{max} for these controllers are 0.0233, 0.0191, and 0.0126 N, respectively. Therefore, the proposed AITSMFC can achieve the best force tracking performance than the other controllers. For a higher frequency 1 Hz in Fig. 8, MFITSMFC still have the largest errors. In contrast, it is found that the proposed AITSMFC achieves the best performance with e_{rms} of 0.0046 N and e_{max} of 0.0177 N. The force tracking errors with the statistical analysis are listed in Table II. It can be

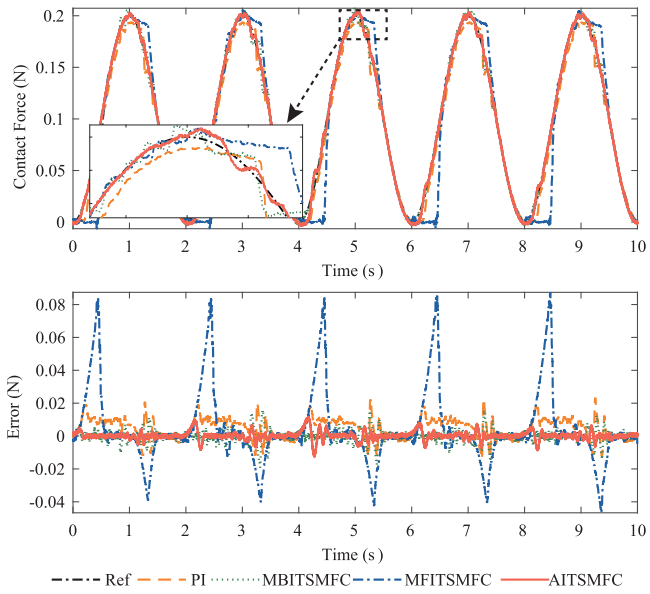

Fig. 7. Experimental results on force tracking at 0.5-Hz sine wave using different controllers.

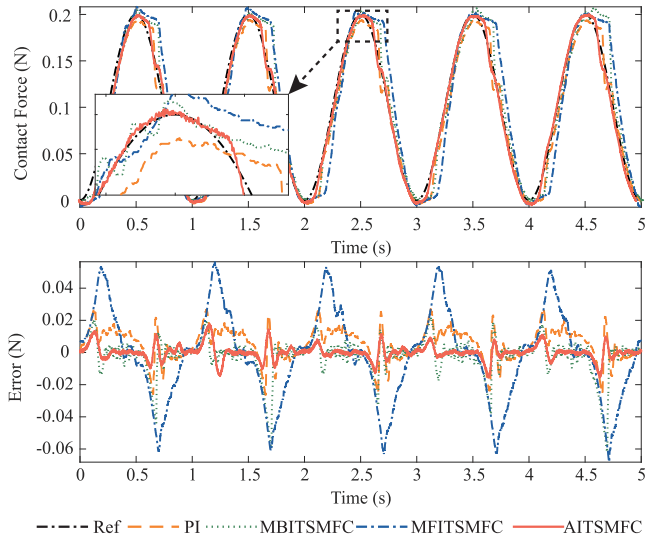

Fig. 8. Experimental results on force tracking at 1-Hz sine wave using different controllers.

TABLE II
STATISTICAL RESULTS OF FORCE TRACKING ERRORS WITH DIFFERENT FREQUENCIES OF SINE WAVES (UNIT: N)

Errors(N)		PI	MBITSMFC Eq. (49)	MFITSMFC Eq. (50)	AITSMFC Eq. (47)
0.2 Hz	e_{rms}	0.0060	0.0083	0.0034	0.0023
	e_{max}	0.0206	0.0426	0.0168	0.0087
	e_{std}	0.0031	0.0082	0.0034	0.0022
0.5 Hz	e_{rms}	0.0079	0.0039	0.0233	0.0026
	e_{max}	0.0233	0.0191	0.0874	0.0126
	e_{std}	0.0064	0.0039	0.0227	0.0020
1 Hz	e_{rms}	0.0113	0.0116	0.0278	0.0046
	e_{max}	0.0278	0.0619	0.0682	0.0177
	e_{std}	0.0099	0.0113	0.0277	0.0046

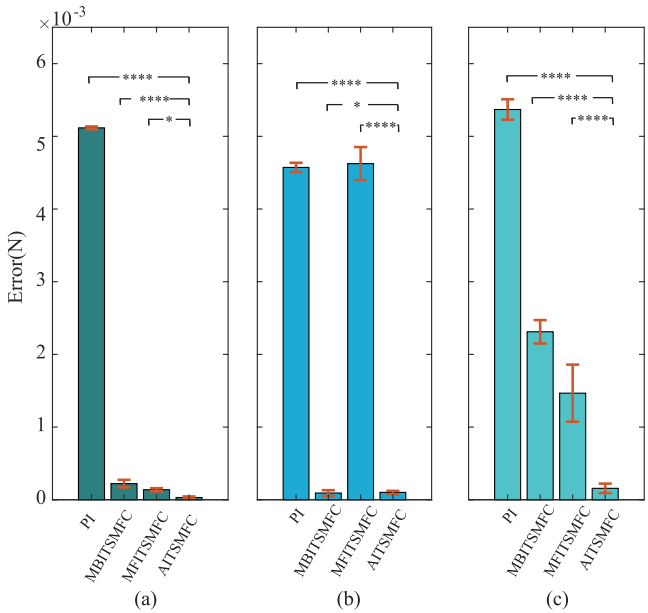

Fig. 9. Error statistical comparisons (mean and standard error of mean) of the four controllers at different frequencies. (a) 0.2-Hz sine wave. (b) 0.5-Hz sine wave. (c) 1-Hz sine wave. *: p-value: ≤ 0.05, ****: p-value: ≤ 0.0001.

concluded that the MFITSMFC can only track low-frequency trajectory, and the force errors of PI as well as MBITSMFC increase with reference's frequencies with a poorer performance in comparison with the proposed AITSMFC.

The error statistical results of different frequencies are illustrated in Fig. 9 for a clear demonstration to facilitate comparison between different controllers. It is observed that PI presents larger mean errors, although with smaller standard deviation (e_{std}) and standard error of mean (e_{sem}), which demonstrates worse steady-state performance, and the other three controllers have similar statistical results. At the condition of 0.5 Hz, MFITSMFC presents the largest mean error and e_{std} at 0.0227 N due the error chattering caused by the friction. The similar phenomenon can also be observed at 1 Hz. For all the conditions, the proposed method achieves the smallest mean error, e_{std} and e_{sem}, and the e_{rms} and e_{max} of AITSMFC are all within 0.0050 and 0.0180 N, i.e., 2.5% and 9.0% of the maximum amplitude. Furthermore, the p-values between AITSMFC and the other three controllers are all less than 0.05 showing significant differences of the tracking performance.

The control efforts of different controllers at 1-Hz sine wave are demonstrated in Fig. 10. It is evident that all the control forces are between -1.6 and $+3.5$ V, which are far below the input voltage range (from -10 to $+10$ V). Moreover, MBITSMFC generates large chattering to compensate the disturbances, especially at the locations with the change of motion direction. Although the control forces of PI control and MFITSMFC are smoother, the force tracking performance is degraded for the low robustness to external disturbances and low tracking ability

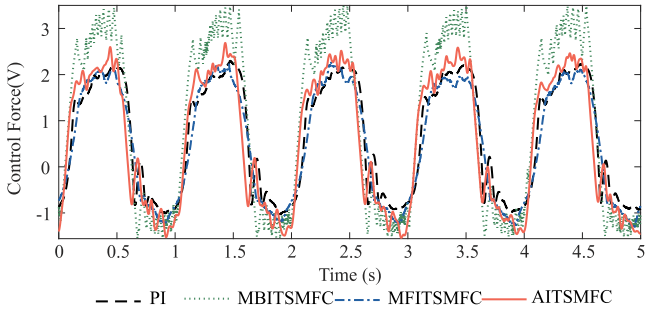

Fig. 10. Control effort of different controllers at 1-Hz sine wave.

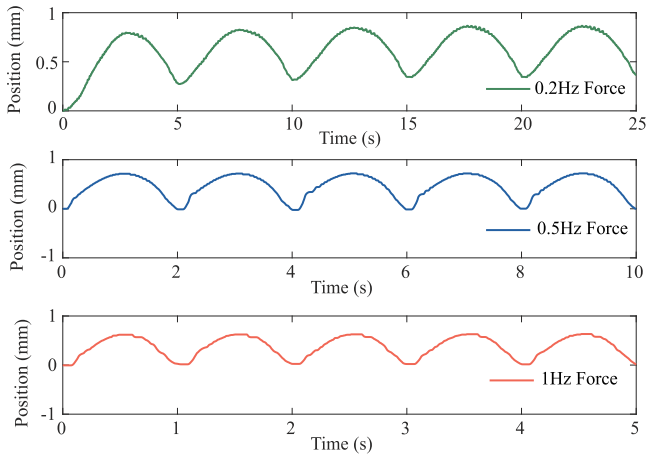

Fig. 11. Measured positions applied on the mock membrane of the AITSMFC at different frequencies.

on the deformable object with the viscoelastic, nonlinear, and inhomogeneous property.

The measured positions applied on the soft deformable mock membrane of AITSMFC at the sine waves of different frequencies are shown in Fig. 11. As mentioned before, the soft membrane, as a deformable object, is usually viscoelastic, nonlinear and inhomogeneous so that the accurate mathematical description is nonlinear [8]. It is also evident from the observation of Fig. 11 that the positions exerted on the membrane are not exactly the same and the insertion depths are varied with the frequencies although the desired forces are standard sine waves. It is noteworthy that the proposed approach can be potentially extended and applied to different types of deformable membranes/objects due to the similar model, such as heart and breast phantom tissues, foam, and so on [11], [12]. Hence, through the proposed method, precision force tracking is achieved without modeling the complex soft interaction.

VI. Conclusion

In this article, to track force trajectories accurately and precisely for a surgical device when it is contacting with the deformable object (e.g., soft TM), an AITSMFC methodology that attains improved effectiveness is proposed. In this control scheme, the integral terminal sliding manifold guarantees the finite-time and fast force convergence, and the controller parameters are updated online through an adaptive law to address the conditions of uncertain or unknown system parameters, disturbances, and to appropriately reduce the chattering phenomenon. The stability and force error convergence of the proposed control method are established and analyzed theoretically based upon the well-known Lyapunov theory and method. Furthermore, representative experiments on the piezoelectric actuator-based ear surgical device are performed for tracking force trajectories contacting with the mock membrane. For the comparative tests conducted, the attained results verify that the best performance on force tracking is achieved by the proposed method comparing with the traditional PI control, MBITSMFC, and MFITSMFC for both S-curve and sine waves with different frequencies. The e_{rms} and $e_{\max}$ of AITSMFC are all within 0.0050 and 0.0180 N, i.e., 2.5% and 9.0% of the maximum amplitude, which achieves the desired force tracking without the requirement of complex modeling of the soft interaction.

In further work, the integration of a position controller, taking into consideration of ear pressure change and other disturbances, will be explored to complete the overall surgery under soft contact. Moreover, the validations of human cadaver experiments and clinical trials will be further investigated.

References

[1] R. H. Taylor, A. Menciassi, G. Fichtinger, P. Fiorini, and P. Dario, "Medical robotics and computer-integrated surgery," in *Handbook of Robotics*. Berlin, Germany: Springer, 2016, pp. 1657–1684.

[2] S. Mansouri, F. Farahmand, G. Vossoughi, A. A. Ghavidel, and M. Rezayat, "Feasibility of infrared tracking of beating heart motion for robotic assisted beating heart surgery," *Int. J. Med. Robot. Comput. Assist. Surg.*, vol. 14, no. 1, 2018, Art. no. e1869.

[3] R. Y. Abdolmalaki, X. Liu, G. J. Mancini, and J. Tan, "Fine orientation control of an insertable robotic camera system for single incision laparoscopic surgery," *Int. J. Med. Robot. Comput. Assist. Surg.*, vol. 15, no. 1, 2019, Art. no. e1957.

[4] J. Kim, S.-I. Kwon, and K. Kim, "Novel block mechanism for rolling joints in minimally invasive surgery," *Mechanism Mach. Theory*, vol. 147, 2020, Art. no. 103774.

[5] K. Hara, Q. Ma, H. Suenaga, E. Kobayashi, I. Sakuma, and K. Masamune, "Orthognathic surgical robot with a workspace limitation mechanism," *IEEE/ASME Trans. Mechatronics*, vol. 24, no. 6, pp. 2652–2660, Dec. 2019.

[6] M. Zhou *et al.*, "Towards robotic-assisted subretinal injection: A hybrid parallel-serial robot system design and preliminary evaluation," *IEEE Trans. Ind. Electron.*, vol. 67, no. 8, pp. 6617–6628, Aug. 2020.

[7] K. K. Tan, W. Liang, L. P. Pham, S. Huang, C. W. Gan, and H. Y. Lim, "Design of a surgical device for office-based myringotomy and grommet insertion for patients with otitis media with effusion," *J. Med. Devices*, vol. 8, no. 3, 2014, Art. no. 031001.

[8] C. Ng, W. Liang, C. W. Gan, H. Y. Lim, and K. K. Tan, "Optimization of the penetrative path during grommet insertion in a robotic ear surgery," *Mechatronics*, vol. 60, pp. 1–14, 2019.

[9] W. Liang and K. K. Tan, "Force feedback control assisted tympanostomy tube insertion," *IEEE Trans. Control Syst. Technol.*, vol. 25, no. 3, pp. 1007–1018, May 2017.

[10] S. Liu, D.-P. Xing, Y.-F. Li, J. Zhang, and D. Xu, "Robust insertion control for precision assembly with passive compliance combining vision and force information," *IEEE/ASME Trans. Mechatronics*, vol. 24, no. 5, pp. 1974–1985, Oct. 2019.

[11] C. Yang, Y. Xie, S. Liu, and D. Sun, "Force modeling, identification, and feedback control of robot-assisted needle insertion: A survey of the literature," *Sensors*, vol. 18, no. 2, p. 561, 2018.

[12] R. Schindeler and K. Hashtrudi-Zaad, "Online identification of environment Hunt–Crossley models using polynomial linearization," *IEEE Trans. Robot.*, vol. 34, no. 2, pp. 447–458, Apr. 2018.

[13] Y. Xie, D. Sun, C. Liu, H. Y. Tse, and S. H. Cheng, "A force control approach to a robot-assisted cell microinjection system," *Int. J. Robot. Res.*, vol. 29, no. 9, pp. 1222–1232, 2010.
[14] C. Liu, P. Moreira, and P. Poignet, "Viscoelastic model based force tracking control for robotic-assisted surgery," in *Proc. 4th IEEE RAS/EMBS Int. Conf. Biomed. Robot. Biomechatronics*, 2012, pp. 1199–1204.
[15] P. Moreira, N. Zemiti, C. Liu, and P. Poignet, "Viscoelastic model based force control for soft tissue interaction and its application in physiological motion compensation," *Comput. Methods Programs Biomed.*, vol. 116, no. 2, pp. 52–67, 2014.
[16] W. Liang, J. Ma, and K. K. Tan, "Contact force control on soft membrane for an ear surgical device," *IEEE Trans. Ind. Electron.*, vol. 65, no. 12, pp. 9593–9603, Dec. 2018.
[17] A. Pappalardo, A. Albakri, C. Liu, L. Bascetta, E. De Momi, and P. Poignet, "Hunt–Crossley model based force control for minimally invasive robotic surgery," *Biomed. Signal Process. Control*, vol. 29, pp. 31–43, 2016.
[18] J. Lee, M. Jin, N. Kashiri, D. G. Caldwell, and N. G. Tsagarakis, "Inversion-free force tracking control of piezoelectric actuatorsusing fast finite-time integral terminal sliding-mode," *Mechatronics*, vol. 57, pp. 39–50, 2019.
[19] Y. Cao and X. Chen, "Disturbance-observer-based sliding-mode control for a 3-DOF nanopositioning stage," *IEEE/ASME Trans. Mechatronics*, vol. 19, no. 3, pp. 924–931, Jun. 2014.
[20] L. Kong, D. Li, J. Zou, and W. He, "Neural networks based learning control for a piezoelectric nanopositioning system," *IEEE/ASME Trans. Mechatronics*, vol. 25, no. 6, pp. 2904–2914, Dec. 2020.
[21] Q. Xu, "Continuous integral terminal third-order sliding mode motion control for piezoelectric nanopositioning system," *IEEE/ASME Trans. Mechatronics*, vol. 22, no. 4, pp. 1828–1838, Aug. 2017.
[22] P. Li, X. Yu, Y. Zhang, and X. Peng, "Adaptive multivariable integral TSMC of a hypersonic gliding vehicle with actuator faults and model uncertainties," *IEEE/ASME Trans. Mechatronics*, vol. 22, no. 6, pp. 2723–2735, Dec. 2017.
[23] J. Y. Lau, W. Liang, and K. K. Tan, "Motion control for piezoelectric-actuator-based surgical device using neural network and extended state observer," *IEEE Trans. Ind. Electron.*, vol. 67, no. 1, pp. 402–412, Jan. 2020.
[24] A. Al-Ghanimi, J. Zheng, and Z. Man, "A fast non-singular terminal sliding mode control based on perturbation estimation for piezoelectric actuators systems," *Int. J. Control*, vol. 90, no. 3, pp. 480–491, 2017.
[25] H. C. Liaw and B. Shirinzadeh, "Robust generalised impedance control of piezo-actuated flexure-based four-bar mechanisms for micro/nano manipulation," *Sens. Actuator A, Phys.*, vol. 148, no. 2, pp. 443–453, 2008.
[26] M. Basin, "Finite-and fixed-time convergent algorithms: Design and convergence time estimation," *Annu. Rev. Control*, vol. 48, pp. 209–221, 2019.
[27] H. Wang, Z. Han, Q. Xie, and W. Zhang, "Finite-time chaos synchronization of unified chaotic system with uncertain parameters," *Commun. Nonlinear Sci. Numer. Simul.*, vol. 14, no. 5, pp. 2239–2247, 2009.
[28] J. Khawwaf, J. Zheng, R. Chai, R. Lu, and Z. Man, "Adaptive microtracking control for an underwater IPMC actuator using new hyperplane-based sliding mode," *IEEE/ASME Trans. Mechatronics*, vol. 24, no. 5, pp. 2108–2117, Oct. 2019.
[29] A. Levant, "Higher-order sliding modes, differentiation and output-feedback control," *Int. J. Control*, vol. 76, no. 9–10, pp. 924–941, 2003.
[30] A. Safa, R. Y. Abdolmalaki, and H. C. Nejad, "Precise position tracking control with an improved transient performance for a linear piezoelectric ceramic motor," *IEEE Trans. Ind. Electron.*, vol. 66, no. 4, pp. 3008–3018, Apr. 2019.
[31] J. Y. Lau, W. Liang, and K. K. Tan, "Adaptive sliding mode enhanced disturbance observer-based control of surgical device," *ISA Trans.*, vol. 90, pp. 178–188, 2019.
[32] P. Ioannou and B. Fidan, *Adaptive Control Tutorial*. Philadelphia, PA, USA: SIAM, 2006.
[33] S. Bashash and N. Jalili, "Robust adaptive control of coupled parallel piezo-flexural nanopositioning stages," *IEEE/ASME Trans. Mechatronics*, vol. 14, no. 1, pp. 11–20, Feb. 2009.
[34] Y. Lee, S. H. Kim, and C. C. Chung, "Integral sliding mode control with a disturbance observer for next-generation servo track writing," *Mechatronics*, vol. 40, pp. 106–114, 2016.
[35] Y. Zhang and P. Yan, "An adaptive integral sliding mode control approach for piezoelectric nano-manipulation with optimal transient performance," *Mechatronics*, vol. 52, pp. 119–126, 2018.
[36] C. Fan, G. S. Hong, J. Zhao, L. Zhang, J. Zhao, and L. Sun, "The integral sliding mode control of a pneumatic force servo for the polishing process," *Precis. Eng.*, vol. 55, pp. 154–170, 2019.
[37] C. Wang, Y. Li, S. S. Ge, and T. H. Lee, "Reference adaptation for robots in physical interactions with unknown environments," *IEEE Trans. Cybern.*, vol. 47, no. 11, pp. 3504–3515, Nov. 2017.
[38] J. Fay, S. Puria, W. F. Decraemer, and C. Steele, "Three approaches for estimating the elastic modulus of the tympanic membrane," *J. Biomech.*, vol. 38, no. 9, pp. 1807–1815, 2005.
[39] J. Aernouts, J. A. Soons, and J. J. Dirckx, "Quantification of tympanic membrane elasticity parameters from in situ point indentation measurements: Validation and preliminary study," *Hear. Res.*, vol. 263, no. 1–2, pp. 177–182, 2010.
[40] L. C. Kuypers, W. F. Decraemer, and J. J. Dirckx, "Thickness distribution of fresh and preserved human eardrums measured with confocal microscopy," *Otol. Neurotol.*, vol. 27, no. 2, pp. 256–264, 2006.
[41] A. Shino, T. Ishii, and M. Takayama, "Measurement of the strength of human tympanic membrane using a force-sensing myringotomy knife," *Otol. Jpn.*, vol. 7, no. 2, pp. 97–101, 1997.

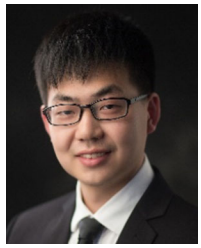

Zhao Feng received the B.S. and Ph.D. degrees in mechanical engineering from the School of Power and Mechanical Engineering, Wuhan University, Wuhan, China, in 2014 and 2020, respectively.

From 2019 to 2020, he was also a visiting Ph.D. student with the Department of Electrical and Computer Engineering, National University of Singapore, Singapore. His research interests include precision control, iterative learning control, nanopositioning, and robotics.

Wenyu Liang (Member, IEEE) received the B.Eng. and M.Eng. degrees in mechanical engineering from the China Agricultural University, Beijing, China, in 2008 and 2010, respectively, and the Ph.D. degree in electrical and computer engineering from the National University of Singapore, Singapore, in 2014.

He is currently a Scientist with the Institute for Inforcomm Research, A*STAR, Singapore and also an Adjunct Assistant Professor with the Department of Electrical and Computer Engineering, National University of Singapore. His research interests mainly include robotics, intelligent systems, precision motion control, and force control.

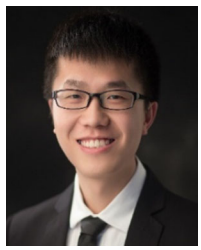

Jie Ling (Member, IEEE) received the B. S and Ph. D degrees in mechanical engineering from the School of Power and Mechanical Engineering, Wuhan University, Wuhan, China, in 2012 and 2018, respectively.

He was a Visiting Ph.D Student with Department of Automatic Control and Micro-Mechatronic Systems, FEMTO-st Institute, Besançon, France, in 2017. From 2019 to 2020, he was a Postdoctoral Researcher with the Department of Biomedical Engineering, National University of Singapore, Singapore. Since 2020, he has been an Associate Professor with the College of Mechanical and Electrical Engineering, Nanjing University of Aeronautics and Astronautics, Nanjing, China. His research interests include mechanical design and precision motion control of nanopositioning stages and micromanipulation robots.

Xiaohui Xiao (Member, IEEE) received the B. S. and M.S. degrees in mechanical engineering from Wuhan University, Wuhan, China, in 1991 and 1998, respectively, and the Ph.D. degree in mechanical engineering from the Huazhong University of Science and Technology, Wuhan, in 2005.

She joined Wuhan University, in 1998, where she is currently a Full Professor with the Mechanical Engineering Department, School of Power and Mechanical Engineering. She has authored and coauthored more than 30 papers in the areas of mobile robots, dynamics and control, and sensors and signal procession. Her current research interests include mobile robotics, high-precision positioning control, and signal processing.

Kok Kiong Tan received the B.Eng. and Ph.D. degrees in electrical and computer engineering from the Department of Electrical and Computer Engineering, National University of Singapore, Singapore, in 1992 and 1995, respectively.

Prior to joining the National University of Singapore, he was a Research Fellow with the Singapore Institute of Manufacturing Technology, Singapore, a national R&D institute spearheading the promotion of R&D in local manufacturing industries, where he was involved in managing industrial projects. He was previously a Professor with the National University of Singapore, and is currently with the ZAI company. His research interests include precision motion control and instrumentation, advanced process control and autotuning, and general industrial automation.

Tong Heng Lee (Member, IEEE) received the B.A. degree (First Class Hons.) in engineering tripos from Cambridge University, Cambridge, U.K., in 1980, and the Ph.D. degree in electrical engineering from Yale University, New Haven, CT, USA, in 1987.

He is currently a Professor with the Department of Electrical and Computer Engineering, National University of Singapore, Singapore. His research interests include the areas of adaptive systems, knowledge-based control, intelligent mechatronics, and computational intelligence.

Dr. Lee is currently an Associate Editor for the IEEE TRANSACTIONS IN SYSTEMS, MAN AND CYBERNETICS; the *Control Engineering Practice* (an IFAC journal); and the *International Journal of Systems Science* (Taylor and Francis, London, U.K.). In addition, he is a past Deputy Editor-in-Chief for *IFAC Mechatronics journal*.